AFRL-RV-HA-TR-2011-1030

Preflight and Vicarious Calibration of Hyperspectral Imagers

Stuart F. Biggar

University of Arizona
1600 E University Blvd, PO Box 210094
Tucson, AZ 85721-0094

Final Report

10 January 2011

AIR FORCE RESEARCH LABORATORY
AIR FORCE MATERIEL COMMAND
Space Vehicles Directorate
29 Randolph Rd.
Hanscom AFB, MA 01731-3010

AFRL-RV-HA-TR-2011-1030

This technical report has been reviewed and is approved for publication.

/ signed /	/ signed /
Steven M. Miller	John C. Holbrook, Chief
Contract Manager	Battlespace Surveillance Innovation Center

REPORT DOCUMENTATION PAGE

Form Approved
OMB No. 0704-0188

1. REPORT DATE *(DD-MM-YYYY)*	2. REPORT TYPE	3. DATES COVERED *(From - To)*
10-01-2011	Scientific, Final	26 Aug 2006 – 14 Dec 2010

4. TITLE AND SUBTITLE
Preflight and Vicarious Calibration of Hyperspectral Imagers

5a. CONTRACT NUMBER
FA-8718-06-C-0012

5b. GRANT NUMBER

5c. PROGRAM ELEMENT NUMBER
62601F

6. AUTHOR(S)
Stuart F. Biggar

5d. PROJECT NUMBER
1010

5e. TASK NUMBER
HS

5f. WORK UNIT NUMBER
A1

7. PERFORMING ORGANIZATION NAME(S) AND ADDRESS(ES) AND ADDRESS(ES)
University of Arizona
1600 E University Blvd, PO Box 210094
Tucson, AZ 85721-0094

8. PERFORMING ORGANIZATION REPORT NUMBER

9. SPONSORING / MONITORING AGENCY NAME(S) AND ADDRESS(ES)
Air Force Research Laboratory
29 Randolph Road
Hanscom AFB MA 01731-3010

10. SPONSOR/MONITOR'S ACRONYM(S)
AFRL/RVBYM

11. SPONSOR/MONITOR'S REPORT NUMBER(S)
AFRL-RV-HA-TR-2010-1030

12. DISTRIBUTION / AVAILABILITY STATEMENT
Approved for public release: distribution unlimited

13. SUPPLEMENTARY NOTES

14. ABSTRACT We developed a calibration plan for a hyperspectral sensor and then designed, built, and calibrated three major instruments to support such calibrations. The instruments included two transfer radiometers, one covering the visible and near infrared using a silicon detector, and another covering the short-wave infrared using a cooled InGaAs detector. The third instrument was an improved model of an autotracking solar radiometer (ASR) that incorporated two, cooled InGaAs detector bands in addition to the typical 10 silicon detector bands of the previous model ASR. The transfer radiometers were delivered to the USAF calibration laboratory. The solar radiometer was used in the field and at the University of Arizona to collect optical depth data for calibration and testing and for the vicarious calibration of ARTEMIS. Prior to the launch of ARTEMIS we made measurements at Kirtland for a preflight radiance calibration. After the launch of the ARTEMIS sensor, we provided vicarious calibration information from a number of field campaigns to assist the USAF in radiometric calibration of the sensor. We used the new ASR (along with an older 10-band radiometer) to collect atmospheric data, and field spectrometers and reference panels to collect ground reflectance data. We then used MODTRAN®5 to compute a top of atmosphere radiance spectrum covering the range of 350 to 2500 nm and provided that, along with the reflectance spectrum of the ground surface and spectral optical depth, to the USAF for the calibration of ARTEMIS. We have continued to use and calibrate the ASR in order to better understand the limitations and use of the additional SWIR bands.

15. SUBJECT TERMS
Hyperspectral imagery Radiometers Multispectral Calibration Vicarious calibration

16. SECURITY CLASSIFICATION OF:			17. LIMITATION OF ABSTRACT	18. NUMBER OF PAGES	19a. NAME OF RESPONSIBLE PERSON
a. REPORT	b. ABSTRACT	c. THIS PAGE	UNL	38	Steven M. Miller
UNCL	UNCL	UNCL			19b. TELEPHONE NUMBER *(include area code)*

Contents

Figures

1. INTRODUCTION

This is the final report on our work to provide support for the preflight and vicarious calibration of hyperspectral imagers for the USAF. During the course of the contract we developed a calibration plan for a hyperspectral sensor and then designed, built, and calibrated three major instruments to support such calibrations. The instruments included two transfer radiometers, one covering the visible and near infrared using a silicon detector, and another covering the short-wave infrared using a cooled InGaAs detector. The third instrument was an improved model of an autotracking solar radiometer (ASR) that incorporated two, cooled InGaAs detector bands in addition to the typical 10 silicon detector bands of the previous model ASR. The transfer radiometers were delivered to the USAF calibration laboratory. The solar radiometer was used in the field and at the University of Arizona to collect optical depth data for calibration and testing and for the vicarious calibration of ARTEMIS.

Prior to the launch of ARTEMIS we made measurements at Kirtland for a preflight radiance calibration. After the launch of the ARTEMIS sensor, we provided vicarious calibration information from a number of field campaigns to assist the USAF in radiometric calibration of the sensor. We used the new ASR (along with an older 10-band radiometer) to collect atmospheric data and field spectrometers and reference panels to collect ground reflectance data. We then used MODTRAN®5 to compute a top of atmosphere radiance spectrum covering the range of 350 to 2500 nm and provided that, along with the reflectance spectrum of the ground surface and spectral optical depth, to the USAF for the calibration of ARTEMIS. We have continued to use and calibrate the ASR in order to better understand the limitations and use of the additional SWIR bands.

2. BACKGROUND

2.1. Vicarious Calibration

We use a reflectance-based calibration method to provide at-aperture radiance data to AFRL in order to determine an in-flight or vicarious radiometric calibration of ARTEMIS. We typically perform such calibration experiments at sites with uniform high reflectance over a large area with clear atmospheric conditions. For the ARTEMIS work we have chosen Ivanpah playa, a dry lakebed in California near the Nevada border on the southeast side of I-10. This area has been used for many “high resolution” civilian sensors such as ETM+ on Landsat 7 and ASTER on Terra. It is large enough for the ARTEMIS sensor, the ground reflectance is fairly high and spectrally flat, the playa is spatially uniform, and there are usually clear sky conditions during spring and fall.

In many cases, vicarious calibration is employed after a rigorous preflight characterization and calibration of a sensor. Once the sensor is characterized for stability, spectral characteristics, and imaging characteristics (MTF and FOV for example), the sensor is usually radiometrically calibrated using a large area, uniform, bright source that

fills the aperture and field-of-view of the sensor. This provides a high quality calibration that becomes the baseline from which changes are determined using either on-board calibration sources or vicarious calibration. In the case of ARTEMIS, various complications made a high quality radiometric calibration infeasible so the vicarious calibration became the only realistic method to provide a calibration of the system.

For other hyperspectral sensors, an integrating sphere or other uniform source with a sufficiently large aperture may be used. As spheres and other sources drift and may not be well calibrated by the vendor, some method of either calibrating the source or validating the calibration is necessary. For this reason, we provided two transfer radiometers as part of the contract.

2.2. Transfer Radiometers

The transfer radiometers are designed to be stable and repeatable. They are rugged to allow for transportation if required. They are designed to measure spheres without adversely loading the sphere by reflecting large amounts of light back into the sphere aperture. They can be used to measure other radiance sources such as a flat diffuser illuminated by a spectral irradiance source (calibrated lamp). The radiometers are custom devices that use some off-the-shelf components such as data loggers, temperature controllers, lock-in amplifiers, choppers, and filters. For these instruments, we chose filter-based designs as they provide better spectral performance as long as the filters are of adequate quality and performance. Filter-based instruments can usually be more sensitive than a grating based instrument as the spectral band pass is typically wider and the detector elements can be larger. We used high quality silicon and InGaAs detectors from Hamamatsu. We chose other equipment that has proven to be reliable in our own radiometers such as a data logger from Agilent. The radiometer's heads are mounted to a heavy-duty tripod that can hold either radiometer.

2.3. Automated Solar radiometer

We designed and built a new solar radiometer for AFRL. This radiometer is based on a previous design for the visible and near infrared but it includes two new channels in the short wave infrared. These channels were included to improve the characterization of the atmosphere at wavelengths longer than those covered by the silicon detectors typically used in most solar radiometers. These two new channels use InGaAs detectors with narrow filters centered at 1250 and 1550 nm. The evaluation of data from these two new channels is more challenging since the atmospheric gas transmittance in the SWIR region is not unity. This requires the view path transmittance for each data point, typically every minute. We use MODTRAN®5 for computing the necessary corrections and the spectral transmittance values are band averaged for the two new channels. The correction is strongly dependent on the particulars of the filters. Custom filters with precisely specified wavelength and edge shapes could reduce the sensitivity to absorption but probably not totally avoid the problem. We have used commercially available off the shelf filters that are in a good but not optimum spectral location.

3. TECHNICAL APPROACH AND RESULTS

3.1 VNIR Transfer Radiometer

The optical design of the VNIR TR in this work is effectively a duplicate of the existing VNIR TR in the RSG laboratory. Details of the mounting of the electronics and the power supplies and data collection equipment are different but functionally the same. The system is operated by LabView code running on a Windows PC. Other improvements over the past version of the VNIR TR include the original data logger model being replaced by an Agilent 34970A due to its higher accuracy and built-in IEEE-488 interface. An automated Sutter filter wheel is implemented rather than the manual filter wheel used in the existing VNIR TR. This allows for automation of the data collection and reduces the possibility of errors associated with manual selection of filters. The Sutter filter wheel power supplies are low noise, linear-pass type designed by Sutter to minimize noise radiated to sensitive electronics like the detector amplifier. A similar wheel has been used in the RSG's VNIR BRDF measurement facility and has worked well when mounted near a detector and amplifier with high gain similar to that required for the VNIR TR.

The detector mount was modified slightly to accommodate improved amplifiers and a different heater design. The radiometer makes use of large-area, windowless Hamamatsu detectors and precision feedback resistors. Military specification electrical connectors are used to reduce noise. Power supplies for the amplifiers are not as low-noise as the original supplies that are no longer available but this is not an issue since uncertainty analysis shows this to be a very small part of the expected error. A key improvement is the development of mechanical drawings using Solidworks which allowed evaluation of parts compatibility prior to assembly and will simplify development of further TRs especially the SWIR version described in the next section.

Selection of spectral filters was based on the original VNIR TR in combination with the expected use of the radiometer in predicting hyperspectral source output. Modeling work done in the previous year showed the filters chosen for the instrument are more than adequate to model the source output. The bands chosen for the radiometer are centered at 413, 443, 489, 552, 672, 746, 801, 874, and 1048 nm. Spectral bands were chosen to span the VNIR while avoiding spectral absorption features.

The VNIR TR was completed during 2007. The work also included the development of a manual for the instrument. The radiometer was part of a series of solar-based calibrations relative to the RSG's other two transfer radiometers. This work and the laboratory characterization results were used in support of two papers submitted to the Annual SPIE meeting held in San Diego in August 2007.

RSG commonly uses a laboratory radiance calibration to characterize transfer radiometers. This method makes use of a standard of spectral irradiance purchased either from NIST or a secondary standards laboratory. The standard is a quartz-halogen lamp rated at 1000 W. The lamp current is actively controlled to match the calibration current

within ± 0.5 mA. The bulb is placed 50 cm from a 25.4-cm Spectralon® diffuser which is measured prior to radiometer calibration using the standard RSG panel characterization method. The illuminated panel is viewed by the transfer radiometer at 45-degrees from the normal. Figure 1 shows the laboratory setup for the radiometer developed as part of this project.

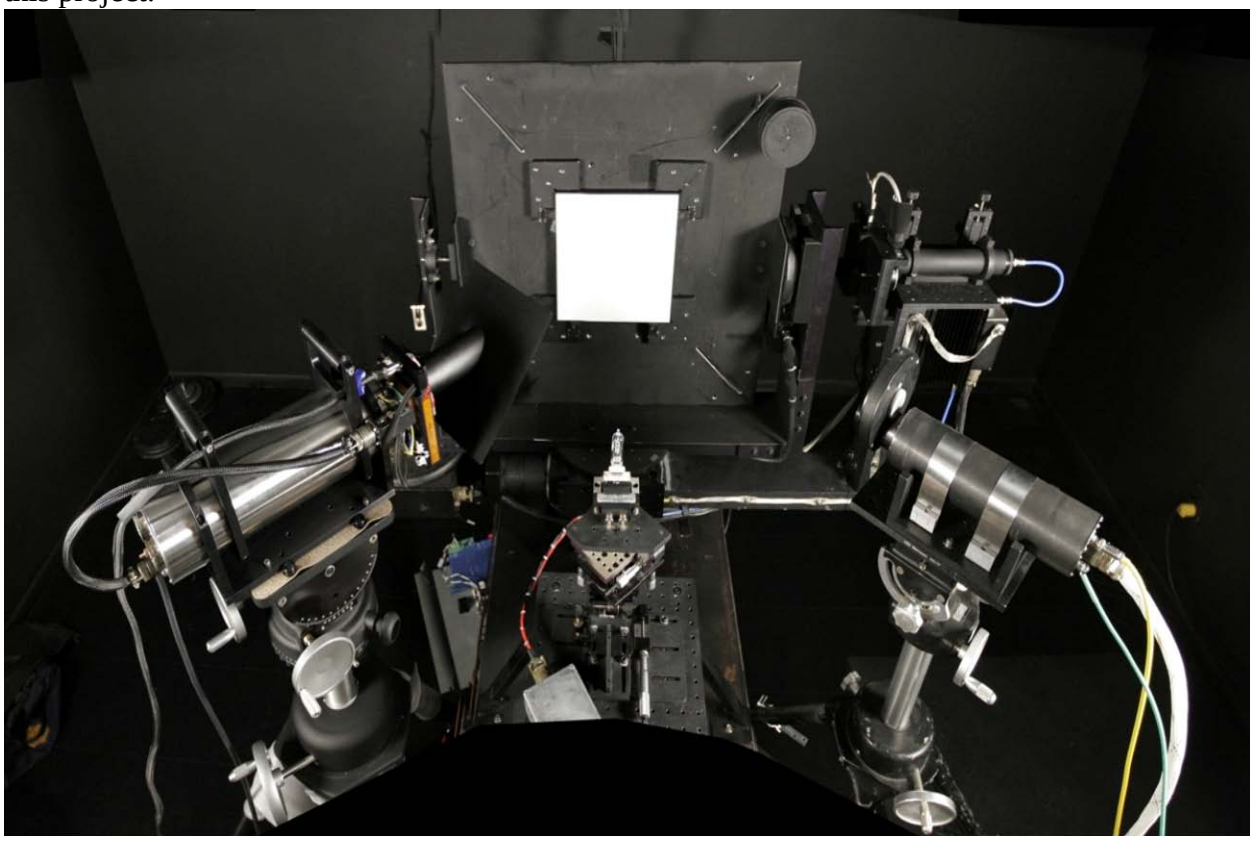

Figure 1. Transfer radiometers with diffuser and FEL lamp

Note the lamp in the center of the setup located 50.0 cm from the panel. The two radiometers in the foreground are transfer radiometers for the current work (left) and UA VNIR #2. They are aligned at 45 degrees from the normal to the panel.

The band-averaged radiance collected by the transfer radiometer in this case is determined based on the given lamp irradiance and the directional reflectance of the reference panel. The band-averaged lamp irradiance is the result of an interpolation of the calibration data provided by NIST with the lamp for the 50-cm distance. The spectral data are generally given in several distinct wavelength increments and are fit with a polynomial-corrected exponential function that is numerically integrated to yield the total irradiance of the lamp in each measurement band.

Repeated measurements on different days of the same source show variations less than 1.0% for all bands. The largest change was found for the 412-nm band where changes in the source are more likely. The change was less than 0.1% for most of the longer wavelength bands; therefore the radiometer-source combination was quite stable.

Multiple measurements of the system noise were also made. The offset signal from the radiometer with the shutter closed was found to be stable at an average of 3.46 millivolts with a standard deviation of less than 2 microvolts for 100 samples. A typical minimum signal when viewing a radiance source is 20 millivolts in the shortest wavelength band and larger for other bands. The geometry shown in Figure 2 leads to signal values between 2000 and 15,000 times the standard deviation of the average for 100 samples. The standard deviation is typically lower when observing a SIS with multiple lamps illuminated. The radiometer is capable of making low noise measurements of typical calibration sources in all bands.

The precision goniometer in our laboratory allows the BRDF of the diffuser in Figure 1 to be determined. Therefore we can compute the panel radiance in the view direction where the uncertainty in the radiance is higher than the irradiance uncertainty due to small geometry errors and the uncertainty in the measurement of the BRDF (estimated to be about 1%).

In addition to the geometry shown above, the radiometer was calibrated by reference to standards of spectral irradiance. The filter, rear aperture, and "trap" detector combination can be calibrated in irradiance units by directly illuminating the back aperture of the radiometer. The front aperture is removed during this calibration. A standard of spectral irradiance (a FEL-type 1 KW halogen lamp in a special bi-post base) was aligned to the radiometer axis at a distance of 100.0 cm from the rear aperture. The lamp irradiance was corrected for the non-standard distance and an irradiance calibration computed from the measurements. As we know the aperture diameters and spacing to high accuracy, we can compute a radiance calibration of the radiometer based on the irradiance calibration and geometry. The expected uncertainty for the lamp calibration is slightly wavelength dependent and less than 1.7% at about 670 nm.

A third method of calibrating the radiometer used the sun as the illumination source. We call this method a solar radiation-based calibration (SRBC). During this calibration we measure the transmittance of the path from the experiment location to the sun with a calibrated solar radiometer. We can then compute the attenuated solar irradiance falling on a Spectralon diffuser. The radiometer views the panel with geometry reciprocal to that in the lab. The radiometer is aligned to view the center of the diffuser along the normal to the panel. The radiometer and panel are rotated together to align the panel to the solar plane. The illumination angle is computed based on time and the solar ephemeris. We correct for the diffuse field by blocking the direct beam to the panel and taking measurements and then taking measurements of the panel when illuminated by both the direct beam and the diffuse field. We may also correct for the small amount of the diffuse field blocked when we block the direct beam if conditions warrant. This experiment yields a radiance calibration for the radiometer where the calibration of the radiometer is then based on the solar irradiance spectrum chosen for the experiment. We typically use the Spectrum published by Thuillier, et al.

The absolute radiometric calibration determined by the two laboratory methods agree to better than 0.5% in all bands. The results from the SRBC approach agree to better than 3% in all bands except 801 and 1048 nm. The SRBC approach was repeated multiple times with several transfer radiometers. The outcomes from averaging multiple SRBC collections from another transfer radiometer were average calibration coefficients ±2.1 % in all bands. The discouraging aspect of the SRBC results is that those from the current radiometer show a consistent negative bias when compared to laboratory calibration.

To verify the repeatability of the laboratory calibration and rule out any resulting effects, the laboratory radiance calibration was repeated with two different calibrated bulbs from two different vendors. The results of this test provided calibration coefficients that agreed to better than 0.65 % in any band. More SRBC collections are certainly necessary to verify their repeatability and accuracy. It is interesting to note that there seems to be very little correlation between the SRBC calibration coefficients and the optical depth of the atmosphere. This leads to the conclusion that barring large amounts of clouds, highly varying atmosphere, or other atmospheric issues, the SRBC is valid as long as accurate and timely atmospheric measurements are performed. Therefore the SRBC should be performed often in lieu of awaiting the "perfect day" of weather.

3.2 SWIR Transfer Radiometer

The SWIR transfer radiometer is an updated design based on what we learned building and using a liquid nitrogen cooled InSb detector instrument for the NASA EOS program. The use of a thermo-electrically cooled detector was investigated to allow use in various orientations and obviate the need for a liquid cryogen. Cooled InGaAs detectors have improved since the EOS radiometer was built so the choice was made to use an off-the-shelf, InGaAs detector from Hamamatsu with sensitivity between 1.2 and 2.5 micrometers. The detector was one of several evaluated that did not require cryogenic cooling. In addition, the chosen detector includes all amplification electronics as part of the detector package. That significantly reduced the risk of incorporating the detector into the radiometer.

The EOS SWIR radiometer used only apertures for defining the field-of-view and no powered collection optics. Unfortunately, the InGaAs detector size, noise, and responsivity required collection optics to ensure adequate SNR at low radiance levels in the SWIR. A reflective design based on commercially available, off-the-shelf optics was designed and modeling gave SNR values comparable to a transmissive design.

Early testing of the detector for the radiometer showed that the offset (no input light) drifted sufficiently with temperature to require a dark-signal measurement during data collection. A chopper approach gives both this measurement as well as the option to collect in AC mode with a limited bandwidth improving the SNR. Thus the design included a chopper that was placed in front of the filter wheel assembly. The limiting aperture for this design became the chopper and the filter wheel.

Spectral filters were selected and ordered based on a genetic algorithm (GA) model used in conjunction with a selection of interpolation algorithms to optimize the filter placement for hyper-spectral curve reconstruction. The choice of interpolation, number of filter samples, and filter placement are the variables used in the optimization. Genetic algorithms are best suited for multi-variable minimization problems wherein the function to be optimized has several local minima. Other minimization methods such as gradient search run the risk of convergence to a local, not global, minimum. The GA, when properly employed, yields a better probability that the final convergence obtained is the global minimum (or maximum). This property of the GA makes it well suited for many types of optimizations. The GA employs the concepts inherent in the process of natural selection, wherein a population of organisms reproduces and evolves in a manner that favors survival of the fittest.

An objective function used to evaluate the quality of the solution in this case is the root summed squared error between the truth curve related to a hyperspectral source and the interpolated reconstruction derived at 1-nm resolution based on multispectral data. The population of individuals is evaluated with the objective function at each iteration (generation) of the GA. Equivalently, an individual may be referred to as a chromosome in GA parlance. As implemented, the population consisted of 20 individuals, a value found to be satisfactory for the performance of the GA; preliminary performance tests allowed up to 50 individuals. In keeping with typical GA terminology, the component filter wavelengths for each individual are referred to as genes. Each individual of n filter samples/radiance measurements within the population may or may not be unique. At each generation, the best individuals are selected by minimizing the objective function. In most applications, these Elite Parents are placed unchanged into the next generation. The next generation is then constructed by assembling randomly selected genes from the elite parents, and a varied number of less optimal parents, into new individuals. A set number of the individuals in the new generation are constructed wholly from this gene set, and the number of new individuals is again a variable parameter of the GA. This set number is fixed for each run of the GA; the set value is often termed crossover.

The remaining individuals in the population are constructed using combined Crossover Parents and randomly selected mutations, new filter positions within the spectral band. The number of mutations and random placements within the individual are drawn from selected probability distributions, using random number generators. If a uniform PDF is implemented, the number of new filter positions is varied between one and the upper bound of the PDF. A Gaussian PDF was found to provide good performance for the filter selection application, also. The number of genes (filters) comprising each individual was varied from eight to as many as 32, with decreasing error as the number of genes was increased. Three different genetic algorithm variations were evaluated, each sufficiently different from the other to allow for different performance.

For the applications intended, the expected calibration radiance curve is a known quantity a priori. Minor variations in the measured curve from the expectation are obtained from the calibration instrument in the field for the MS or HS application. The measured variations are the result of different conditions in the calibration source at the time of

calibration. The radiance sub-band expectation, the 'truth' curve, is available to the user of this method. Three interpolation algorithms were investigated for this effort. The three interpolators were cubic spline, PCHIP (Piecewise Cubic Hermite Interpolating Polynomial), and Bulirsch-Stoer rational function interpolation. Each of these interpolators is optimal for specific functional curve forms. The cubic spline and PCHIP returned the best results; the Bulirsch-Stoer interpolation algorithm consistently returned the largest error regardless of the sub-band applied, required an order of magnitude more processing at each interval, and frequently resulted in singularities of the rational function denominator.
Nearly universally, the PCHIP interpolator returned the minimal reconstruction error to all sub-bands investigated (SWIR, VNIR, full-spectrum). On the other hand, the cubic spline interpolator proved more robust to reconstruction of a severely perturbed set of measurements. The cubic spline interpolator frequently paired filter placement in regions of the curve where the slope was changing, equivalently where the second derivative of the spectrum was large. The GA approach was applied to the SWIR range from 1.0 to 2.5 micrometers. The residual error decreased in an asymptotic manner as the number of filter samples increased to the upper limit of 20 filter samples. The objective function had a value less than 0.08% of the total integrated SWIR radiance. The GA results indicated that minimal improvement was seen beyond 12 filters. The objective function has a value of 1.07% for eight filters that decreases to 0.22% for twelve samples. Given that the best approximation at twenty samples returns an error of 0.08%, the twelve-sample configuration has eliminated 78% of the residual error difference between eight and twenty samples. The filter wheel selected for the SWIR TR has only 10 openings. The best ten-sample set positioning returns a relative reconstruction error of 0.43%, or 57% of the possible improvement gained by increasing filter samples from eight to twenty.

The error as a function of wavelength in reconstructing the hyperspectral output of the sphere source based on the bands selected for the radiometer is shown in Figure 2 (below). The bands were selected based on the spectral range of the selected InGaAs detector combined with only allowing commercially available filters. The center wavelength of the filters selected are at 1200, 1319, 1455, 1500, 1648, 850, 1945, 2050, 2190, and 2285 nm. The total error for the objective function is 0.42%, thus little accuracy in the curve fit is lost when restricting the operating range of the TR.

After the filters were selected and the radiometer constructed, testing was done to quantify performance. One issue arose in that the linearity of the system was found to be suspect at low radiance levels as shown in the plots in Figure 3. Deviation from linear is on the order of 5-15% for the points shown in the lower figure (the same points can be seen in the lower left corner of the upper plot). The impact of these results is that careful use of the neutral density filters must occur to optimize the SNR while not creating non-linear effects at low radiance. Error as a function of wavelength between the reconstructed, hyperspectral output from the sphere source was compared to the actual source output. The reconstruction is based on the 10 spectral bands selected for the SWIR TR.

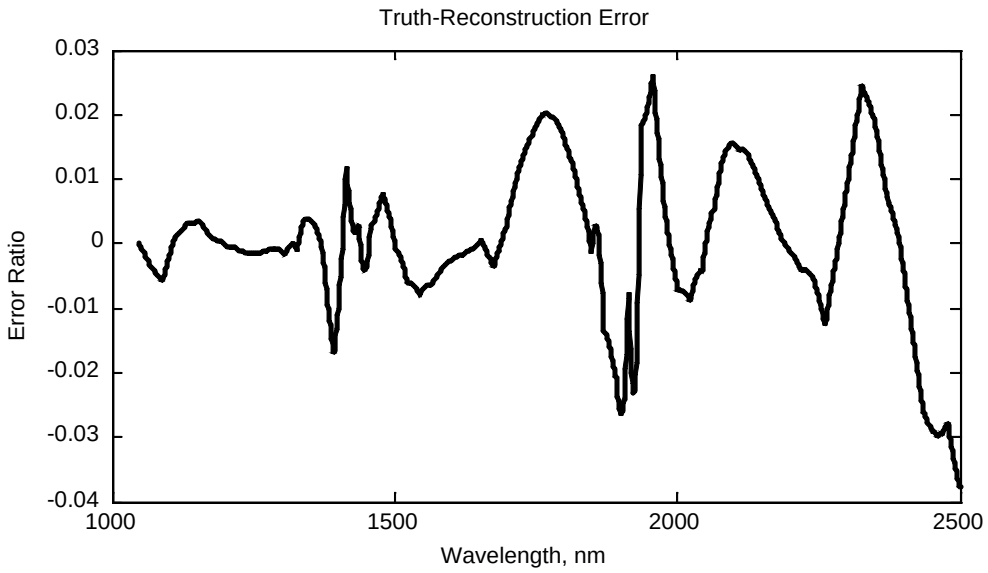

Figure 2. Reconstruction Error

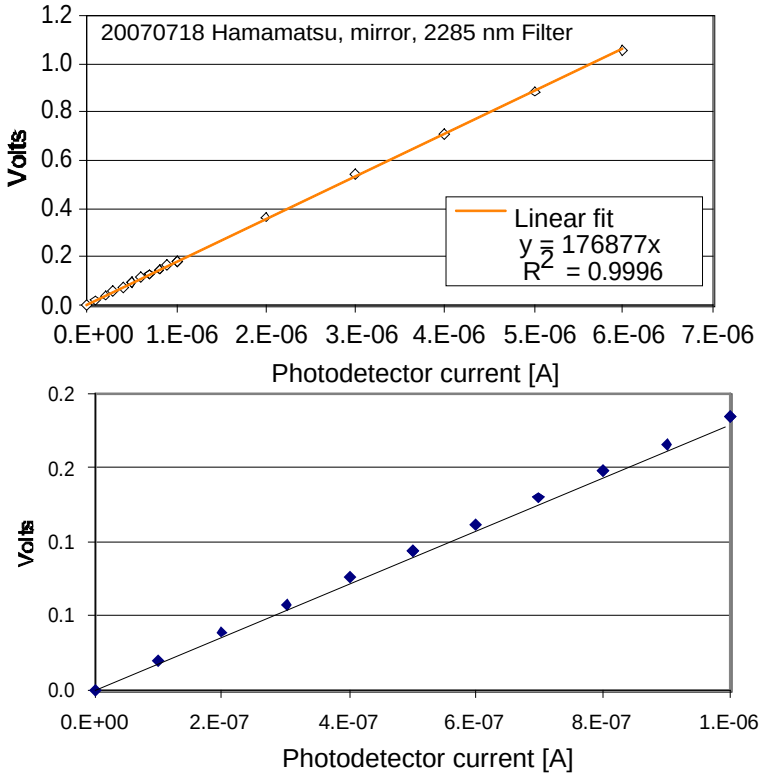

Figure 3. Linearity study results from SWIR TR detector

The spectral filters for the instrument were characterized in a fashion similar to that of the VNIR instrument. The process was complicated by the RSG's move to a new laboratory facility and due to a malfunctioning monochromator. The completion of the filter characterization allowed for the completed assembly of the instrument. The radiometer is shown in Figure 4. The chopper for the system is the dark box to the right and shows the

off-angle mounting designed to reduce stray light. The fan on top of the device removes heat from the TE-cooled detector (black box with two cable connected to top). The filter wheel is also clearly visible between the detector package and chopper.

Initial testing of the radiometer relied on the RSG's small, radiance stabilized sphere with the band pass filter centered at 2285nm. Comparisons between the data from this measurement to the predicted sensor output based on model values helped determine the selection of neutral density filters for all bands. The average radiometer output was below the saturation level at a value of 1.035 V with a standard deviation of 60 microvolts. The dark reading was an average of 85 microvolts with a standard deviation of 40 microvolts. The inferred SNR based on these data is 17,250 and this showed RSG that the system was behaving as designed.

The completed system was calibrated by reference to the EOS transfer radiometer, as the goniometer normally used was not available because of a move from a flooded, off-campus facility to an on-campus laboratory.

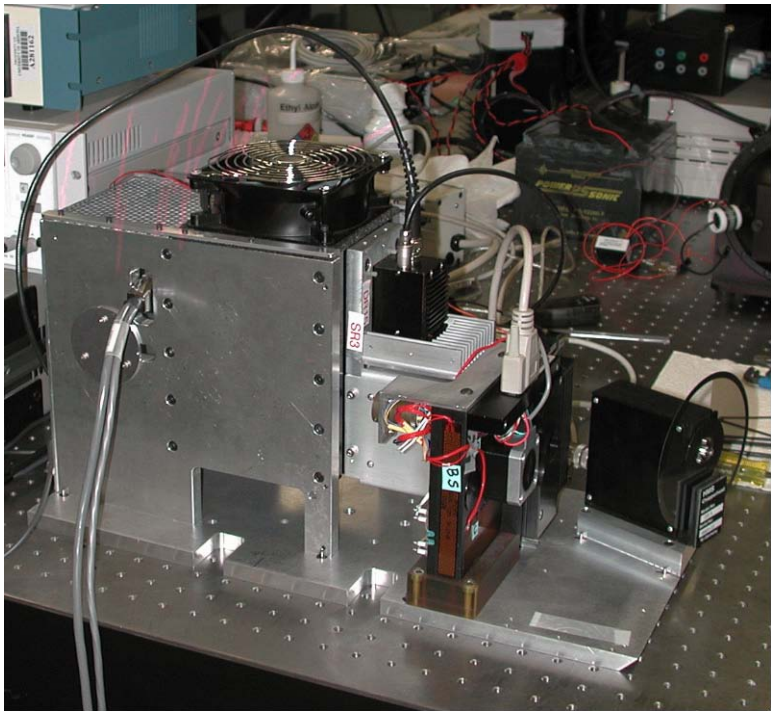

Figure 4. SWIR Radiometer in testing (covers removed)

3.3 Automated Solar Radiometer

We completed the design and construction of a 12-band automated solar radiometer. This instrument builds on the older 10-band design by adding 2 bands in the SWIR and adding a barometer, temperature and relative humidity sensor, and GPS receiver. The two SWIR bands were added to improve the characterization of the aerosols at longer wavelengths. The barometer adds pressure into the data stream to allow for more accurate estimation of the molecular scattering component. The GPS is used to set the clock for the data logger and controller so the time of data collection is known more accurately. This is important for accurate measurements at low sun angles. The GPS should also allow for inclusion of the ASR location into the data stream but the GPS board level device we installed has not so far given accurate location information.

We developed a new processing scheme for the two SWIR channels, as there is some residual absorption in the SWIR bands even though they are narrow and were chosen to avoid obvious absorption features. We had issues when we used MODTRAN®4 for correction; the results with MODTRAN®5 are better as the absorption has been updated in the SWIR. We presented a poster at Calcon covering the new solar radiometer. We are using the radiometer and refining the calibration, especially in the SWIR. Data from the radiometer during an ARTEMIS calibration experiment are shown in Figure 5 below.

We have also completed some additional characterization of the radiometer. One test done outside using the sun as the source was a measurement of the effective field-of-view of each spectral band. The radiometer was set to track the sun and then the tracking was stopped while data were collected. Over time, the sun moved away from the optical axis of the stopped radiometer. The relative response of each band as a function of angle from on-axis is shown as Figure 6. Ideally, the field of view would fall off very sharply for many orders of magnitude. However, in the SWIR the field of view is not as well defined as it is for the VNIR. This is probably due to a reflection from the inner wall of the cylinder holding the detector, filter, and aperture. The performance shown in the SWIR is, however, sufficient to allow useful data in the SWIR, as there is only a small signal at longer wavelengths in the solar aureole.

Recently we have carefully studied the uncertainty we expect with the ASR measurements. The basic uncertainty comes from instrument limitations such as the drift of the amplifiers and the measurement errors of the digitizer. Further errors result from the computation of the effects of molecular scattering and the absorption by gasses such as ozone and water vapor. The ASR measures transmittance to the sun. For use with MODTRAN®5 and other atmospheric correction codes, we need to partition the transmittance to allow us to infer the aerosol component. We then model the aerosol with some assumptions that add further uncertainty.

For the radiometer itself, we expect an uncertainty in the intercept of about 0.2% (or better) in the VNIR bands if the conditions are near perfect. There is an expected uncertainty of about 0.25% in computing the contribution of molecular scattering based on the measured pressure and various factors involved in the computation. There is an

uncertainty of about 3% in the column amount of ozone that is used to compute the absorption due to ozone. Once we correct for molecular scattering and absorption that leaves us with an estimate of the aerosol contribution that is modeled using a Junge fit. In the end, we estimate that our transmittance measurements are no worse than 1.5% uncertain except in areas of strong absorption by variable components like water vapor.

Based on the study, we expect that ASR measurements used to guide MODTRAN®5 to predict transmittance should give values within 1.5% of the actual value. For ASR measurements to characterize an atmosphere for vicarious calibration, the top-of-atmosphere radiance modeling is more uncertain. The major uncertainty is not from the inputs derived from the ASR but rather from the uncertainty in the surface reflectance. This is especially true for the type of atmospheric conditions typically encountered in the Southwest US during calibration experiments where the visibility is very high and the aerosol loading is very low.

We have attempted a number of Langley calibration attempts with the new ASR. Figure 7 shows the history. The break in the traces at the start of 2010 marks a move from unipolar digitization (positive voltages only) to bipolar digitization to allow for measuring and then correcting for negative offsets. As the digitizer is capable of 15-bits plus sign in bipolar mode, the loss of resolution is negligible compared to the expected uncertainty in the intercept or the individual measurements. Bipolar mode allows for a more accurate offset correction for the bands where the measured voltage with zero illumination is negative. We now measure the offset at the beginning and end of a data collect and during the collect as other duties allow. Figure 8 shows the offset and temperature of the SWIR channels during use. This figure is typical. In general, the offset is about 1% of the change in signal in the SWIR channels over a data collect so the correction for the offset results in a more accurate intercept value in the SWIR. The offset is smaller as compared to the signal change in the VNIR but correcting for the offset will allow us to more closely approach the expected uncertainty in the intercept. The water vapor band is much more variable so the intercept and uncertainty are much larger than for the other bands. Also, as water vapor absorption exhibits saturation, the typical Langley method cannot be used so a square root method is used instead.

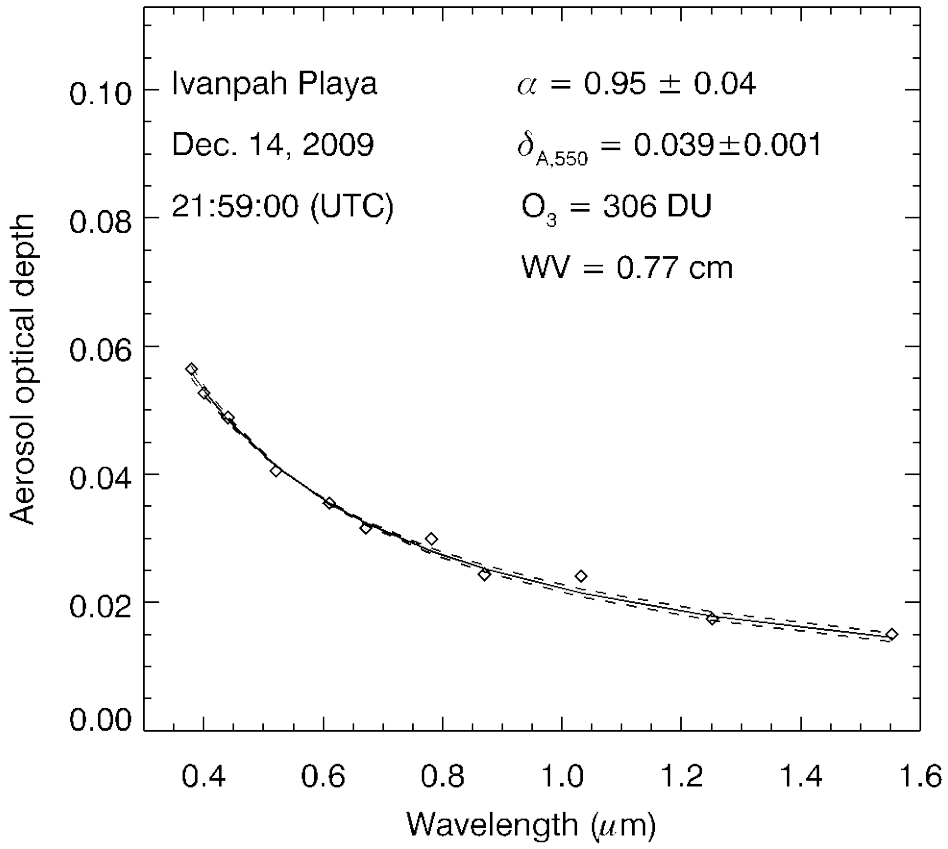

Figure 5. Aerosol optical depth as determined using ASR-33 including SWIR bands

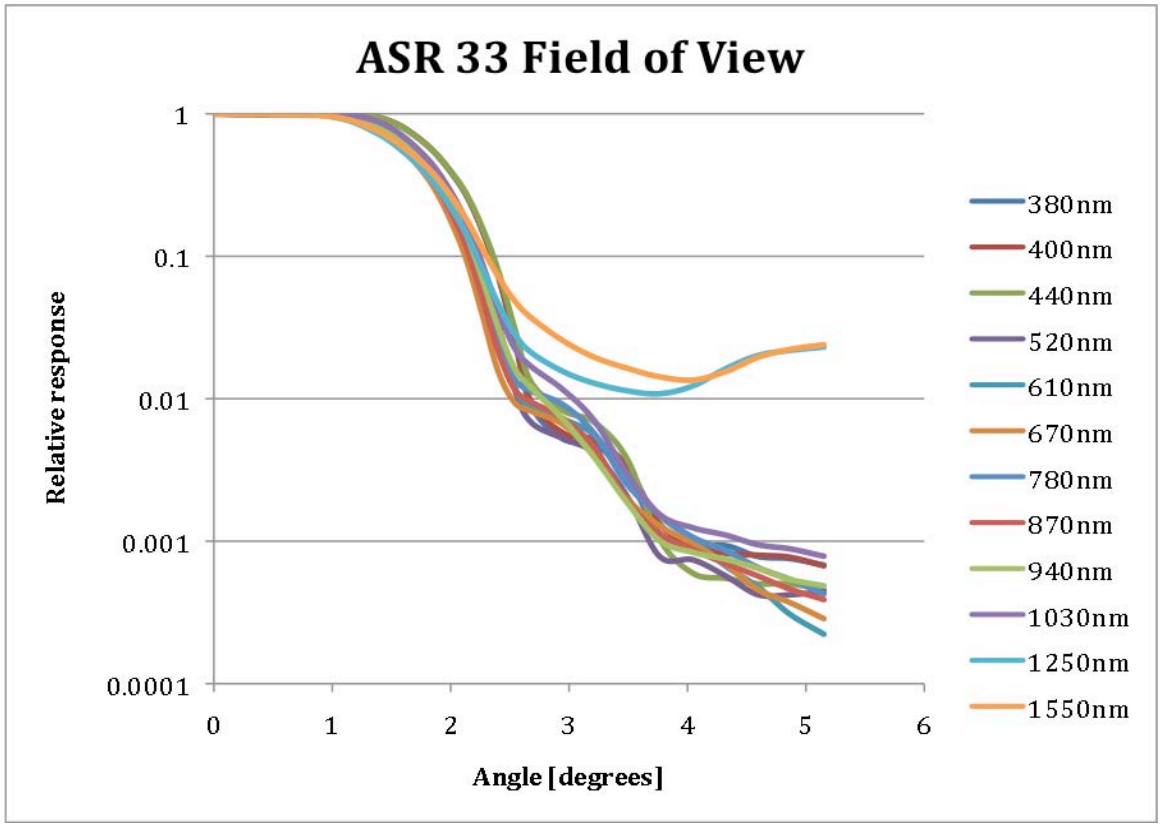

Figure 6. ASR 33 field of view

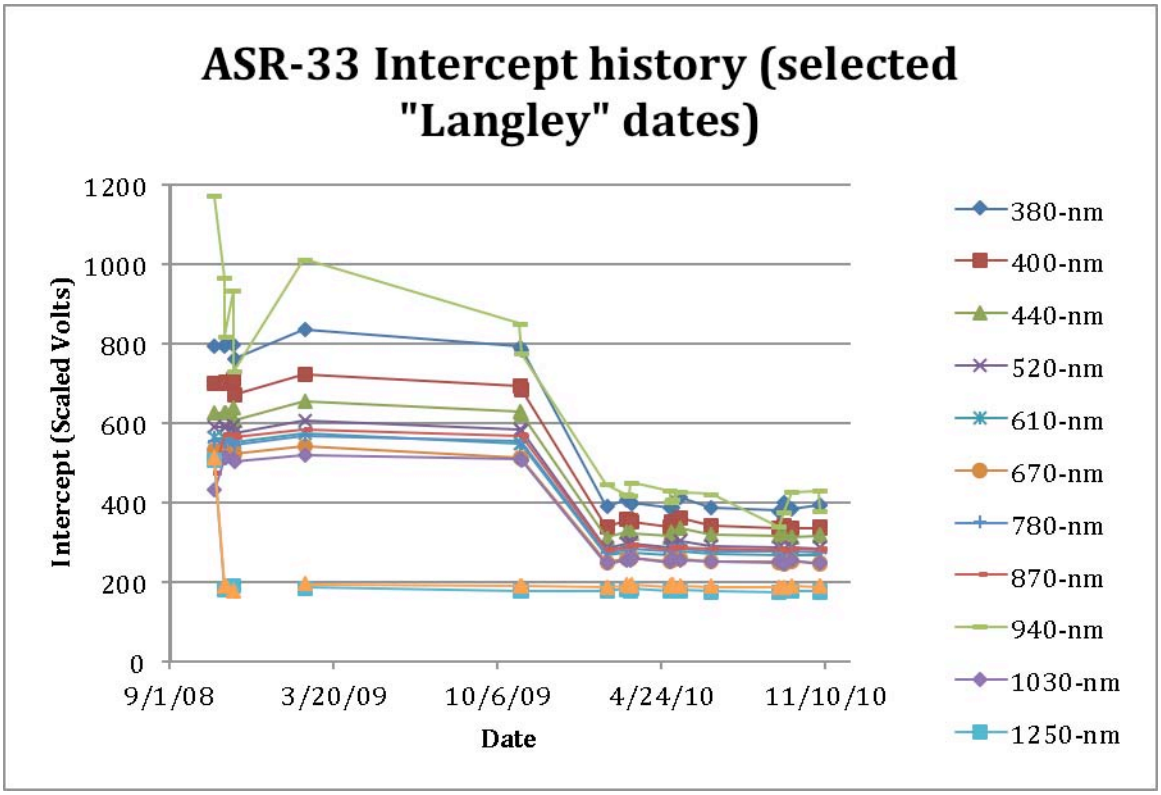

Figure 7. ASR-33 intercept history (selected "Langley" dates)

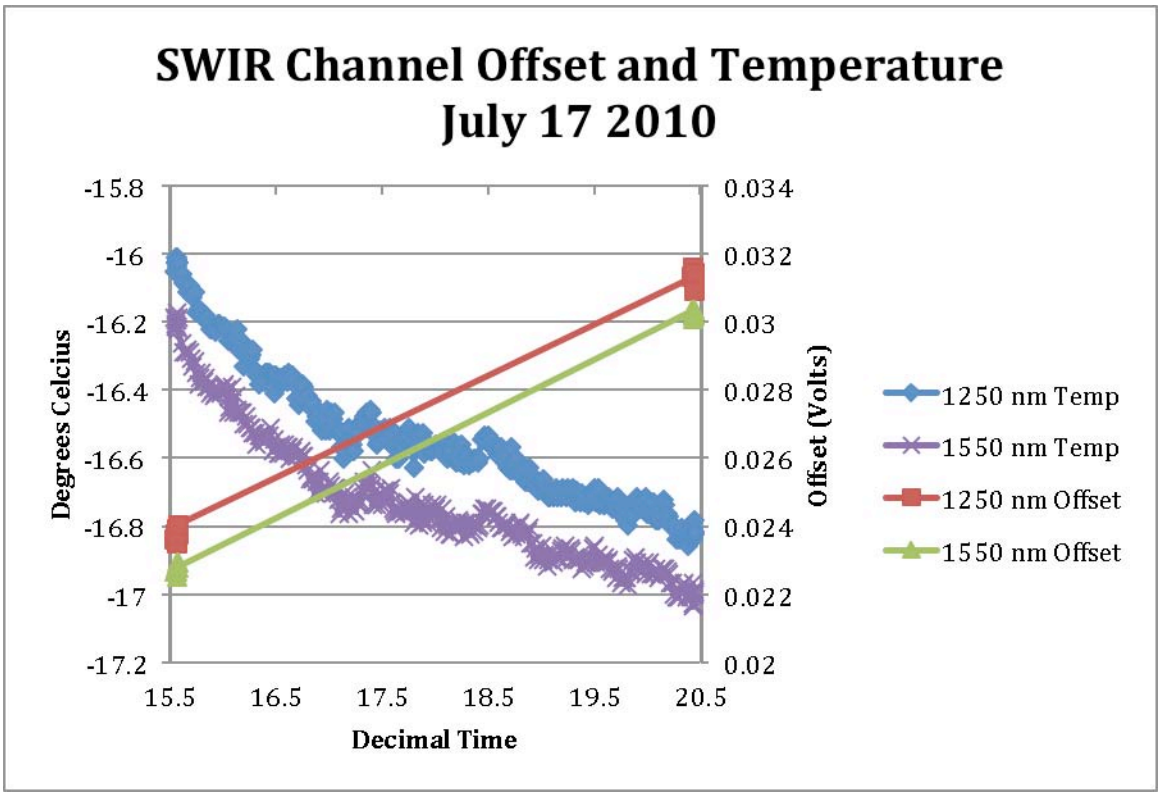

Figure 8. SWIR channel offset and temperature July 17 2010

3.4 MODTRAN®5

We evaluated the beta version of MODTRAN®5 and are now using the released version with ARTEMIS spectroscopy. We have helped with some debugging of run time errors (NaN) with a couple of different compilers on UNIX (Solaris) and Windows. We are now using MODTRAN®5 running under Solaris 10 SPARC (Sun fortran compiler) and Windows (Intel fortran compiler for Windows). The results from each platform are very close but not exactly the same. We are now using MODTRAN®5 for correcting our ASR data for absorption in the SWIR. We have recently verified that the results from MODTRAN®5 built with the Intel compiler on Apple OS X is consistent with the version built with the Intel compiler on Windows.

3.5 Preflight calibration of ARTEMIS

The goal of the calibration is to predict the at-sensor radiance on the entrance pupil of the ARTEMIS system at hyperspectral intervals to allow a determination of the calibration of ARTEMIS in all bands not affected by strong absorption. Three methods were originally planned though the final approach relies only on the direct measurement of the radiance incident on ARTEMIS using a VNIR and SWIR transfer radiometer (TR) as well as a hyperspectral radiometer. The other two methods were not implemented because the large solar zenith angles for the experiment required knowledge of the orientation of the

reference to better than 0.5 degrees to limit the uncertainty from geometry to less than 1.8%. There was no readily available method to align the panel to this accuracy, so no attempts were made to rely on knowledge of the panel BRDF.

The method used for ARTEMIS relied on a set of well-calibrated radiometers to assess the spectral radiance at the entrance aperture of ARTEMIS. One advantage to a transfer radiometer approach is that it allows for a straightforward traceability to national standards. The key advantage to the transfer radiometer approach is that it negates the need to understand the atmospheric transmittance, diffuse light component, and panel BRDF that are part of the signal from a sunlight illuminated diffuser. The lack of a relay system to bring the sunlight onto the aperture of ARTEMIS greatly simplifies the problem and reduces uncertainties.

Measurements for the SRBC data collections began with an attempted Langley calibration collection of the solar radiometer. Unfortunately, cloud conditions prevented the successful collection of these data and conversion of the raw solar radiometer data that were collected relied on previously obtained calibration data. The uncertainty of the solar radiometer calibration was less than 0.3% in precision and 1% in "absolute" calibration. For this work, the solar radiometer uncertainty does not impact the final uncertainty of the predicted at-ARTEMIS radiance. The data from the solar radiometers primarily provide an estimate of the temporal variability of the atmospheric conditions.

The combination of solar zenith angle and azimuth difference between the sun and ARTEMIS panel meant that the smallest zenith angle on the panel would be about 62 degrees for the April 7 collection. Weather forecasts on that day and other scheduling issues prompted the SRBC of ARTEMIS to take place as soon as feasible resulting in solar zenith angles on the panel between 62 and 68 degrees. Time constraints and weather forecasts permitted only a single attempt on April 7. Sky conditions during the period were clear, with morning clouds that prevented the Langley calibration of the solar radiometers dissipating by 15:30 UTC. Sky images are available for the full period.

The two TRs were calibrated in the laboratory after the campaign and were calibrated using an SRBC approach prior to the ARTEMIS work. The same calibration approach was used with the ASD Full Range. The positioning of the radiometers was driven by the VNIR TR that has an FOV that is approximately 4 degrees, full field and the SWIR FOV that is somewhat larger. Thus, the radiometers had to be within 14 m of the large ARTEMIS reference to ensure that its FOV is filled. A closer position was selected to help reduce out-of-field effects and reduce errors from alignment. The ASD FR and SWIR TR were collocated with the VNIR TR for simplicity of operation. The collection procedure was determined by the timing of the VNIR and SWIR TR, since the current RSG TRs use manual filter wheels. The direct-radiance experiment began with the TRs being cycled through all spectral bands while viewing the ARTEMIS reference from a perpendicular view that is aligned with ARTEMIS. The ASD FR also collected data throughout this entire period. The goal is to assess the radiance from an identical view as that expected by ARTEMIS to remove BRDF effects. The length of time for this collection was 6 minutes from start of collection.

After completion of the perpendicular-view data, the transfer radiometers were moved as rapidly as feasible to a marked location for the subsequent radiance tests. ARTEMIS collected radiance data from the reference panel soon after the transfer radiometers were moved. The transfer radiometers and ASD started collection about 12 minutes after the on-axis data. The ASD continually collected data from the ARTEMIS reference during the entire transfer radiometer collection. The SWIR and VNIR#1 were cycled through their spectral bands as done above, taking approximately 6 minutes. This was repeated. The shaded/unshaded SRBC data collection was followed by a repeat of the perpendicular view collection.

Other data sets that were collected included an SRBC of RSG VNIR#2 TR, an SRBC of the ASD, meteorological data, all-sky images, and the solar radiometer data. The SRBC of the RSG TRs is identical to that for ARTEMIS itself except using an RSG reference.

The dominant error source for the ARTEMIS SRBC is the absolute uncertainty of the calibration of the radiometer used for determining the at-ARTEMIS radiance. The choice was made to rely on the field spectrometer data as this permits direct comparison of spectra with the ARTEMIS imagery. The results provided were 1-minute averages of the field spectrometer results. Temporal variability of the spectrometer data over the 1-minute time period is <0.3% in the VNIR and <0.5% in the SWIR. Averages over longer periods gave similar standard deviations. The time averaging also served to reduce the noise in the SWIR bands.

Assessment of the absolute uncertainty is derived through comparisons between the multispectral and hyperspectral radiometers. Figure 9 shows the results comparing the measurements of the three radiometers. The multispectral data are the singular data points for a given measurement in a given band from the first set of on-axis measurements. No attempt has been made to correct for temporal effects since the impact should be <1%. The field spectrometer data sets shown are an average over the 6-minute time period corresponding to the multispectral data set. The qualitative agreement between the laboratory transfer radiometers is quite good. Quantitative analysis of the difference between the field spectrometer and laboratory radiometers is shown in Figure 10. The comparisons used values for the nominal center wavelengths as well as 5-nm rectangular band averages. Data from the 940 and 1380 channels are omitted due to the strong water vapor absorption affecting the SNR of the instruments and difficulties of comparing sensors due to the strong spectral variability in these bands.

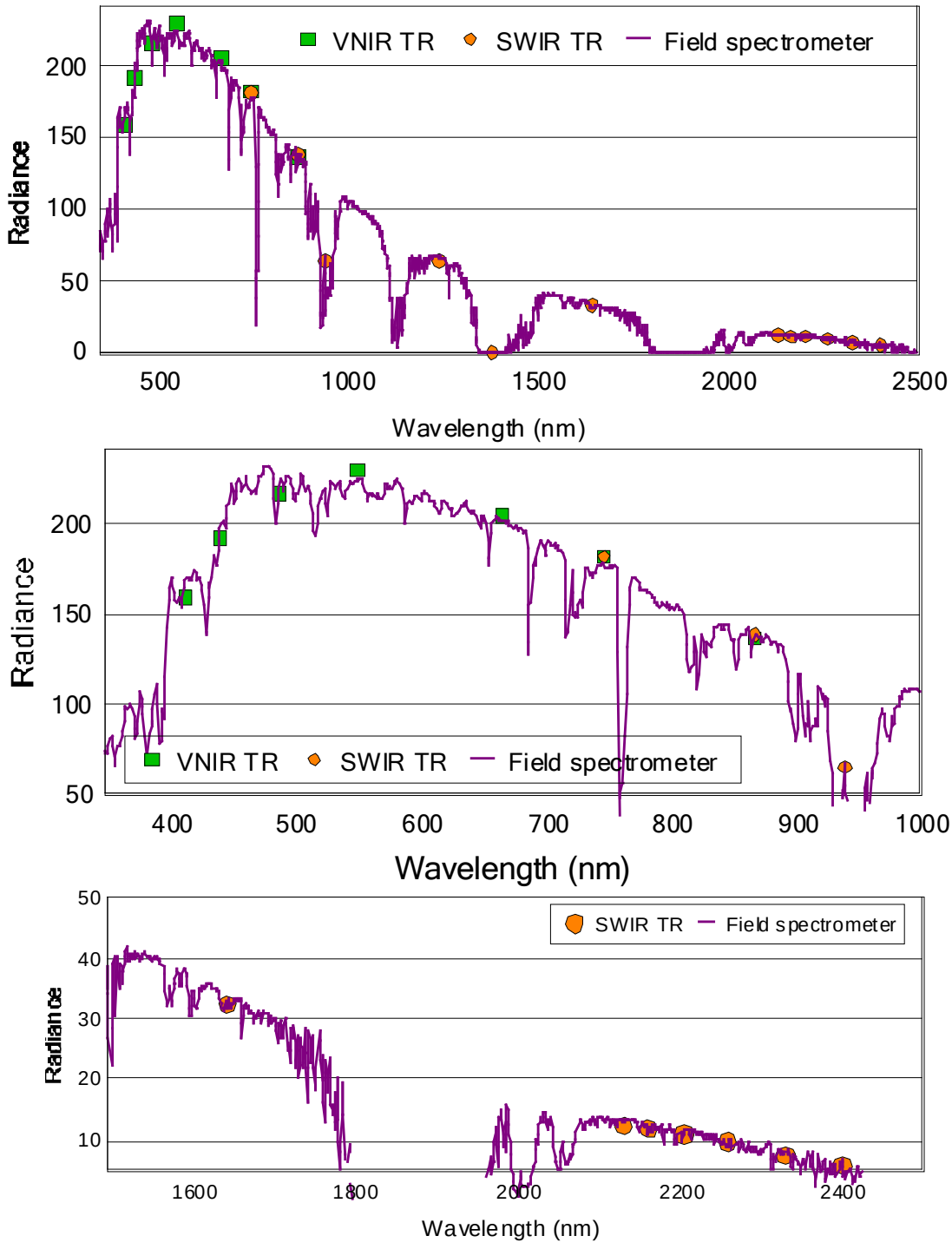

Figure 9. Spectral radiance from the first set of on-axis measurements

The results in Figure 10 show that the agreement between the radiometers is better than 3.7% for all bands <1700 nm. Spectral averaging effects are largest at shortest wavelengths as expected and inclusion of the actual spectral bands of the multispectral radiometers should improve the comparisons. Larger differences are seen in the SWIR between the multispectral and hyperspectral measurements. A portion of this difference is due to the fact that field spectrometer has been calibrated using an SRBC approach while the multispectral radiometer is calibrated relative to a lamp source. There are consistent biases seen in the SRBC and lamp results. Figure 11 shows the bias seen in the VNIR bands between a laboratory-based and SRBC-based calibration. The results shown in the figure are an average of five dates of data collected at a variety of locations. Note that the values are reasonably consistent with the differences seen between the field spectrometer and transfer radiometer in Figure 10.

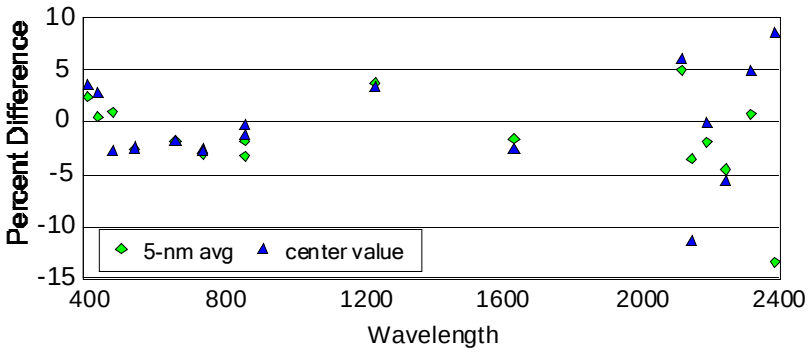

Figure 10. Differences between hyperspectral and multispectral

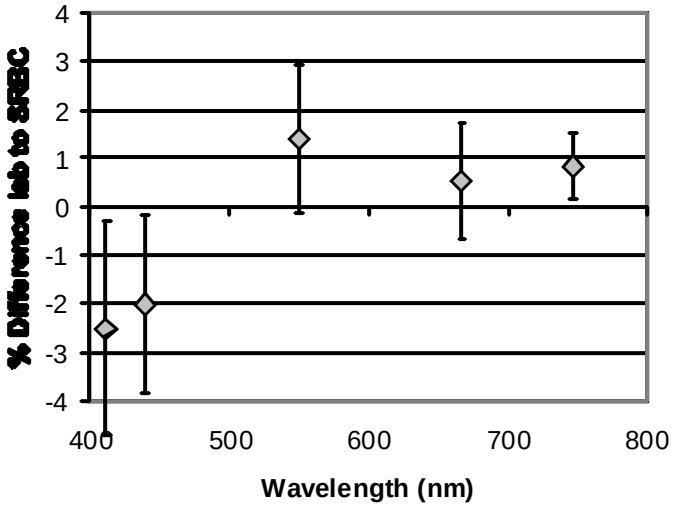

Figure 11. Bias between laboratory and SRBC calibrations, VNIR TR

The at-ARTEMIS radiances provided by RSG are those measured by the ASD FR6014 averaged to 1-minute intervals measured from an off-axis position at times during which ARTEMIS viewed the reference on axis. The ASD data were selected because it directly provides the necessary bands without need for interpolation. The data from the ASD are converted to spectral radiance using calibration coefficients derived from an SRBC done in Tucson shortly before the work in Albuquerque. Laboratory calibration data were not available due to the lack of facilities from the RSG's move to campus. One advantageous outcome of using the SRBC calibration of the ASD is that the use of a consistent solar model between the ASD and the conversion of ARTEMIS radiance to reflectance will reduce the absolute uncertainties in the SWIR present due to the choice of solar model.

The use of the ASD data negates the need to know the reference reflectance, its orientation, and atmospheric transmittance. Diffuse-light and stray light effects would be only those factors between spectrometer and ARTEMIS and are assumed to be negligible. The primary error source then becomes the absolute uncertainty in the field spectrometer's calibration.

Work with other sensors shows that uncertainty in the SRBC calibration of the ASD relative to a given solar model is 1.4% in the SWIR and 2.2% in the blue. The precision and repeatability of the ASD has been shown not to be of the same quality as a laboratory-grade transfer radiometer. However, time and spectral averaging of the data from the spectrometer improved SNR to a level that the above uncertainties are

reasonable as a best case. Laboratory-based calibration uncertainties are similar in the VNIR but significantly larger in the SWIR due to uncertainties in the lamp outputs. RSG work indicates that the calibration of its SWIR transfer radiometer ranges from 3-5% in absolute radiometric uncertainty. Thus, the conservative estimate of the absolute uncertainty of the at-ARTEMIS radiance values are 2% in the 400-1000 nm spectral range and 5% in the 1000-2500 nm spectral range. Uncertainties in spectral regions for which the slant path transmittance is <0.8 are significantly larger than this.

3.6 In-flight calibration of ARTEMIS

Since the launch of ARTEMIS on TacSat 3, we have made a number of field trips to Ivanpah Playa to collect ground data to perform a reflectance-based vicarious calibration of ARTEMIS. For these calibrations, we need a dry lakebed, clear skies, and a collected image. We have made many attempts (at Ivanpah unless otherwise noted):

09/06/01	
09/06/02	
09/06/03	
09/06/04	
09/06/05	
09/07/21	
09/07/22	
09/07/23	
09/07/24	
09/07/27	Alkali Lake – first success
09/09/01	
09/09/02	
09/09/09	good weather
09/09/10	good weather, full swath collect
09/10/28	poor
09/10/29	good
09/11/08	good except clouds at end of ground collect
09/11/09	
09/12/14	good
10/01/01	cirrus
10/04/16	cirrus, clearing during overpass

We typically (over many years) have about a 50% success rate but we have done much worse than that with ARTEMIS, especially in June and July.

For days where the sky was clear and an image was acquired, we measured the ground reflectance of the site using an ASD FieldSpec Full Range portable spectrometer. We used a Spectralon panel (18”x18”) that was calibrated in our laboratory as a reflectance standard. We also measured a 48% reflectance doped Spectralon panel to verify instrument operation. We compensate for the solar zenith angle at the time of measurement using the measured BRDF of the Spectralon. The result is a measured

reflectance spectrum covering the spectral range of 350 to 2500 nm, the range of the ASD.

During the actual collection, we carry the spectrometer over a series of transects covering an area of about 320 meters by 90 meters. The sequence of Spectralon and playa measurements takes about 40 minutes to complete and the start time is chosen such that the scheduled image collection falls near the middle of the reflectance collection. We collect a large number of samples of the playa spectra and the reduced spectrum is an average of the area measured. We mark two corners of the measured area of the playa with blue tarpaulins so the measured area of the playa can be found in the ARTEMIS image.

We have also done two full swath collections where the ASD was carried over a transect corresponding to the full swath of the ARTEMIS sensor. This data was processed in blocks so the data could be averaged to provide a better estimate of the reflectance.

During the entire reflectance collection, the solar radiometer collects transmittance data along the path from the radiometer to the sun. The radiometer is typically started early in the morning and operates until after the reflectance data are collected. We also collect ancillary data such as temperature, atmospheric pressure, radiance along the estimated line-of-site to the ARTEMIS sensor, and total irradiance falling on a diffuser. These data are combined with the transmittance data to determine the total, molecular, and aerosol optical depths for each radiometer channel. We estimate the column amount of ozone based on the measurements and the column amount of water vapor. From the spectral optical depth of the aerosol component, we estimate the particle size distribution of the aerosols and use that to model the scattering phase function. This phase function, the optical depth components, water vapor and ozone, along with the reflectance spectrum, are used as inputs to MODTRAN®5 to compute the estimated top-of-atmosphere radiance for the sensor when viewing the playa.

We provide the measured reflectance spectrum, computed radiance spectrum, and atmospheric data to AFRL. AFRL personnel extract the average digital counts for the area of the image for each band and then determine a calibration based on the spectra and the counts.

An example of the measured reflectance of Ivanpah playa and the resulting top-of-atmosphere radiance are shown as Figures 12 and 13 below.

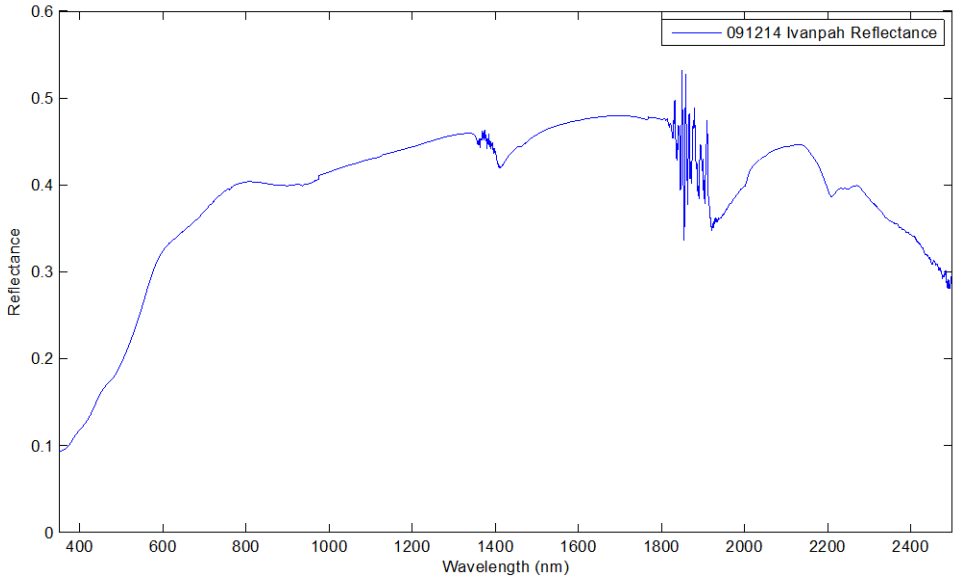

Figure 12. Ivanpah reflectance on 2009 December 14

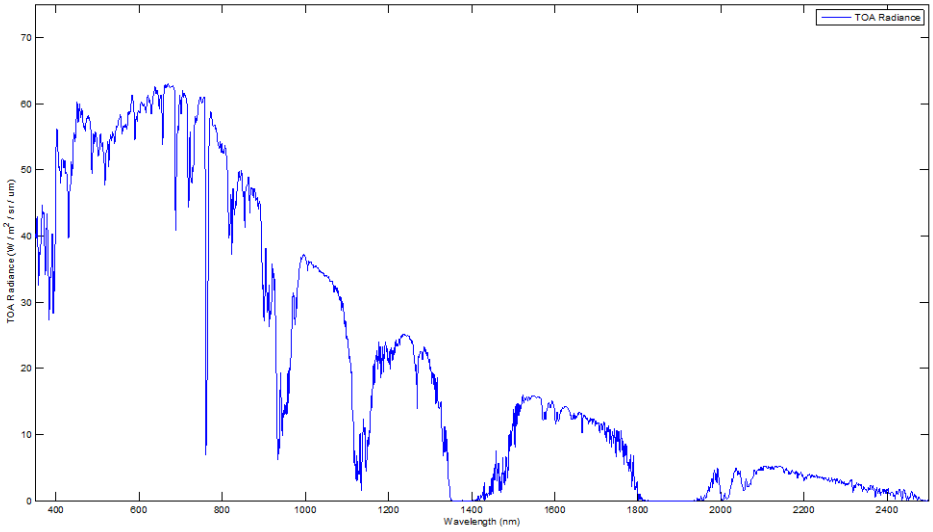

Figure 13. Ivanpah top-of-atmosphere radiance on 2009 December 14

3.7 Cross-calibration of ARTEMIS to MODIS

Joel McCorkel developed a method for using MODIS imagery over North Africa to provide a cross-calibration of ARTEMIS to MODIS. He provided appropriate top-of-atmosphere radiance values derived from MODIS measurements of the same area on the ground at similar illumination and view geometries. This method was described in his PhD dissertation that was defended during the 4th year of the contract. Joel used Hyperion data in his dissertation but supplied ARTEMIS results to AFRL.

3.8 Measured reflectance of panels at Ft Huachuca

We have completed numerous measurements of all the targets installed at Fort Huachuca, at least two reflectance collections per target. For this work we used an ASD FieldSpec FR and a Spectralon reference panel. We built a new, small reference as we found the heavy casings and supports made it difficult to move our large (18"x18") field Spectralon panels over some areas at the Fort. The small reference was calibrated in the lab in the same way as our larger panels. For a few dates where the sky was not clear, we used a reflectance attachment probe for the ASD that includes an internal lamp source. Hyperspectral reflectance data for each target measured were provided to AFRL. We made nine trips to measure reflectance during 2009: Feb 19, Apr 2, Apr 9, Apr 29, May 14, Jul 18, Jul 30, Oct 26, and Nov 6. We made eight additional trips in 2010.

We have measured two particular panels on multiple dates. The reflectance data for various dates are shown in Figures 14 and 15 below. Note that the data from 20090718 and 20091106 were taken with the probe. We normally take 4 samples when using Spectralon and the sun and 8 samples with the probe. However, each of the 4 samples is a spatial average of one side of the panel as the spectrometer is moved during the scan. The probe is stationary at each sample and the area sampled optically is much smaller using the probe. The standard deviation using the sun and Spectralon is between 2% (visible) and 5% (SWIR past 2000 nm) and higher when using the probe (> 10% for 400 nm to about 2% at about 600 nm and up to about 8% past 2000 nm). The higher standard deviation using the probe is probably due to a lower signal from the lamp in the probe and also due to the limited spatial sampling when using the probe, as the area measured is small and is probably not an adequate estimate of the average for the entire surface.

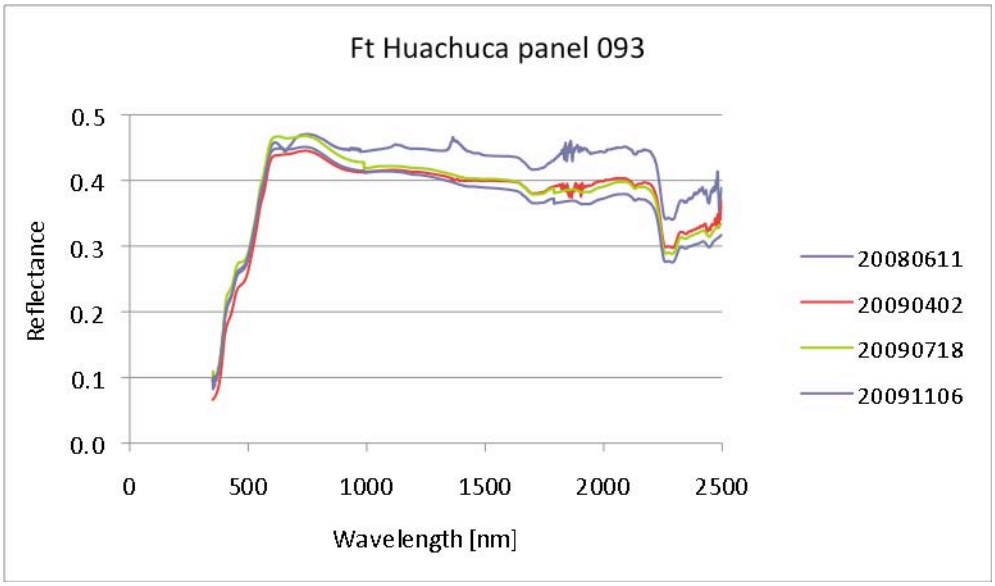

Figure 14. Panel 93 measured reflectance

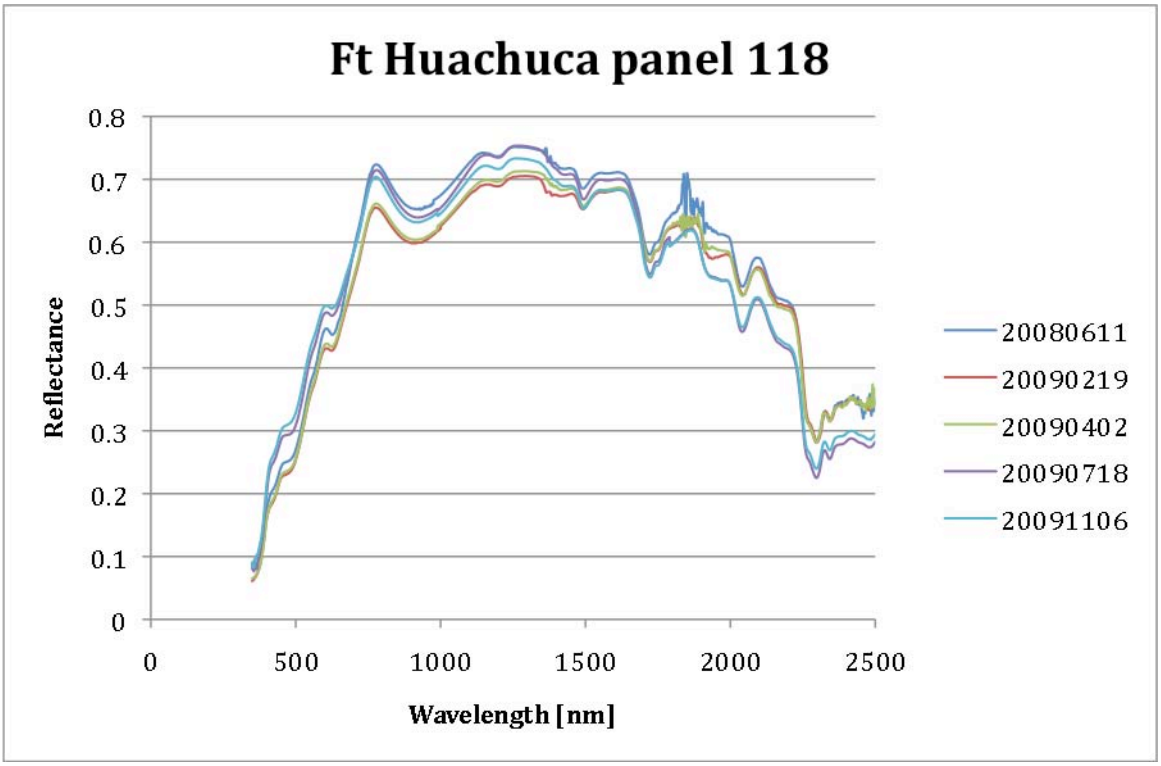

Figure 15. Panel 118 measured reflectance

4. DISCUSSION

We have provided instruments for the USAF AFRL remote sensing calibration laboratory to help with the radiometric calibration of hyperspectral instruments. We have designed, built, and calibrated a new solar radiometer with SWIR bands. We have used this new radiometer to collect data for hyperspectral sensor calibrations of ARTEMIS. We are also using it to study the accuracy of our atmospheric characterization and the limits of the instrumentation and data reduction.

We have provided radiance data to allow AFRL people to compute both the preflight and in-flight vicarious radiometric calibration of ARTEMIS. The multiple, in-flight data sets are especially important since there is no on-board calibration system. We have provided measured reflectance values for each of the field reflectance panels installed at Ft Huachuca in southeast Arizona. This set of reflectance data should allow for a good comparison with atmospherically corrected ARTEMIS data. We have used the new 12-band ASR to collect atmospheric data that extends into the SWIR. The new instrument gives us more confidence in our estimates of aerosol effects in the SWIR and shows that our aerosol model is appropriate for our ARTEMIS calibration experiments

Based on our work, we have some suggestions for improvements to the hardware we provided. For the solar radiometer, we expect that the performance in the SWIR region would be improved by using a chopper and lock-in amplifier. This would reduce the

effects of drifting, zero-signal offsets that are probably due to temperature changes over the period of data collection. Better temperature control of both the silicon and InGaAs detector assemblies would also improve performance at wavelengths longer than about 900 nm and for the shortest wavelength. Better-specified (and probably expensive) custom filters in the SWIR could allow for less absorption in the SWIR ASR bands. As we need to correct for the absorption, better control of the passband of the filters would reduce the size of the correction and improve the accuracy of the transmittance measurement by the radiometer. Moving from MODTRAN®4 to MODTRAN®5 has improved the absorption correction for the existing filters but avoiding more of the absorption would be better. Another possible improvement could come from investigating any absorption correction for the VNIR ASR filters. They were chosen to avoid absorption in general but some improvement to the data for extremely clear days might be possible with absorption corrections in the VNIR.

We have purchased a higher quality (military specification but without the cryptologic components) GPS receiver for the ASR but it has been backordered. This should allow for accurate position reporting but we have not been able to integrate it yet.

The wavelength coverage of the transfer radiometers could be improved by adding more filters of different wavelengths. The existing filter wheel in each instrument can be modified and combined with another wheel in series to allow for up to 18 filters per instrument. More filters would allow for better matching of any spectral features in the source being measured. In the SWIR instrument, the additional wheel could be used instead for the neutral density filters that are now inserted manually. This could allow for more automated data collection in the future.

5. STUDENT SUPPORT

During the period of the contract, two students did research toward their dissertation that was useful for this contract. Jim Keef worked on the methods for estimating the output of an integrating sphere based on a number of measurements in finite spectral bands such as those taken by a filter-based transfer radiometer. This problem is not easily solved as the sources in the sphere are difficult to accurately model and the sphere effective throughput is strongly dependent on the wall reflectance of the sphere. The non-ideal directional reflectance characteristics of the sphere coating (and coated baffles or obstructions inside the sphere) further complicate the model. The sphere modeling work was combined with the measured spectral output of the sphere to determine a good set of spectral filters for the transfer radiometers, especially in the SWIR region. These filters allow for a fairly accurate reproduction of the measured sphere output. However, certain features such as the regions affected by water vapor are not well modeled. The title of Keef's dissertation was "Hyper-Spectral Sensor Calibration Extrapolated from Multi-Spectral Measurements".

Joel McCorkel researched using a well-calibrated filter-based instrument to calibrate a hyperspectral instrument. He evaluated using MODIS to calibrate Hyperion in his dissertation research but he applied the same method to calibrate ARTEMIS. This method is useful over areas where the surface reflectance is stable in time and the areas are large in extent so that using a low spatial resolution sensor such as MODIS (nominal 1 km pixels) is feasible. This method can be used whenever there is nearly coincident imagery from both sensors. Corrections for sun and view angle differences make the results usable over a range of times. McCorkel's dissertation was titled, "On-orbit characterization of hyperspectral imagers".

Other students worked on the calibration and use of both the transfer and solar radiometers, gaining experience with new research instruments.

Bibliography

Nik Anderson, Stuart Biggar, Kurt Thome and Nathan Leisso, (2007) "Solar radiation-based calibration of laboratory grade radiometers", Proc. SPIE 6677, 66770X; doi:10.1117/12.740146

Nik Anderson, Kurt Thome, Stuart Biggar and Jeffrey S. Czapla-Myers, (2008) "Design and validation of a transfer radiometer", Proc. SPIE 7081, 708104; doi:10.1117/12.795478

Nikolaus J. Anderson, Stuart F. Biggar, Jeffrey S. Czapla-Myers, Joel T. McCorkel, Nathan P. Leisso, Ronald B. Lockwood, and Thomas W. Cooley, 2009 "Design and Testing of an Upgraded Automated Solar Radiometer with TE-cooled SWIR Channels," Poster, 18th Annual CALCON Technical Conference, Logan, Utah.

Stuart F. Biggar, Kurtis J. Thome, Ronald B. Lockwood and Steven Miller, (2007) "VNIR transfer radiometer for validation of calibration sources for hyperspectral sensors", Proc. SPIE 6677, 66770W; doi:10.1117/12.740231

Keef, J. L. (2008), Hyper-Spectral Sensor Calibration Extrapolated from Multi-Spectral Measurements, Tucson, Arizona: University of Arizona.

McCorkel, J.T., and Thome, K. J., (2008) "Cross-calibration of hyperspectral imagers using multispectral sensors, " Proc. 17th Annual CALCON Technical Conference, Logan, Utah.

Joel McCorkel, Kurt Thome, Nathan Leisso, Nikolaus Anderson and Jeff Czapla-Myers, (2009) "Radiometric characterization of hyperspectral imagers using multispectral sensors", Proc. SPIE 7452, 745210; doi:10.1117/12.828608

McCorkel, J. (2009), On-orbit Characterization of Hyperspectral Imagers, Tucson, Arizona: University of Arizona.

Kurtis J. Thome, Ronald B. Lockwood, Stuart F. Biggar, Nik Anderson, Jeff Czapla-Myers, Steven J Miller, Thomas G. Chrien, Stephen J. Schiller, John F. Silny, Mary Ann Glennon and Thomas W. Cooley (2008), "Preflight and Vicarious Calibration of ARTEMIS," Geoscience and Remote Sensing Symposium, IGARSS 2008, doi: 10.1109/IGARSS.2008.4778840

Acronyms and Abbreviations

AC	Alternating Current
AFRL	Air Force Research Laboratory
ARTEMIS	Advanced Responsive Spectrometer
ASD	Analytical Spectral Devices, Inc. (instrument manufacturer)
ASR	Autotracking Solar Radiometer
ASTER	Advanced Spaceborne Thermal Emission and Reflection Radiometer
BRDF	Bidirectional Reflectance Distribution Function
CALCON	Name of Conference on Characterization and Radiometer Calibration for Remote Sensing
EOS	Earth Observing System (NASA program)
ETM+	Enhanced Thematic Mapper Plus – a sensor on Landsat 7
FEL	ANSI designation for a 1000 Watt quartz halogen bi-post lamp
FOV	Field Of View
FR6014	ASD FieldSpec Full Range instrument, Serial number 6014
GA	Genetic Algorithm
GPS	Global Positioning System
HS	HyperSpectral
InGaAs	Indium Gallium Arsenide
mA	milliampere
MODIS	Moderate Resolution Imaging Spectroradiometer
MODTRAN	Moderate resolution atmospheric Transmission
MS	Multi-Spectral

MTF	Modulation Transfer Function
NaN	Not a Number
NIST	National Institute of Standards and Technology
nm	nanometer
PCHIP	Piecewise Cubic Hermite Interpolating Polynomial
PDF	Probability Distribution Function
RSG	Remote Sensing Group (College of Optical Sciences, University of Arizona)
SIS	Single Integrated Source
SNR	Signal-to-Noise Ratio
Solaris	UNIX operation system variant by Sun Microsystems (now Oracle)
SPARC	CPU architecture from Sun Microsystems (now Oracle)
SRBC	Solar Radiation-Based Calibration
SWIR	Short-Wave InfraRed
TE	Thermo-Electric
TR	Transfer Radiometer
UTC	Coordinated Universal Time
VNIR	Visible and Near InfraRed
W	Watt